BIS ENERGY AND ENGINEERING

Volume 2 2025 | DOI: 10.31603/biseeng.209
6th Borobudur International Symposium on Science and Technology (BIS-STE) 2024

UNIMMA PRESS
UNIVERSITAS MUHAMMADIYAH MAGELANG

Minimizing distortion in flux cored arc welding of A36 steel by preheating and its effect on weld mechanical properties

Bela Amelia[1], Mochammad Noer Ilman[1*], Nur Akhmad Triwibowo[2]

[1] Department of Mechanical and Industrial Engineering, Faculty of Engineering, Universitas Gadjah Mada (UGM), Yogyakarta, Indonesia
[2] Institut Teknologi Dirgantara Adisutjipto (ITDA), Yogyakarta, Indonesia
[*] Corresponding author email: ilman_noer@ugm.ac.id

Abstract

Welding technology is one of the joining processes that is widely used in-ship industry, but it faces some challenges such as distortion and residual stress due to local heating. Welding distortions can affect the precision and appearance of ship structures. This study aims to reduce welding distortion through preheating and its influence on weld mechanical properties, including strength and hardness are evaluated. Welding processes were conducted on ASTM A36 steel plates using flux cored arc welding (FCAW) and E71T-11 filler metal. Welding parameters used including welding current, arc voltage and speed were 110 A, 20 Volt and 1.5 mm/s respectively. Preheating treatments were applied by heating both sides of the weld using electric heater bands at various temperatures of 100, 200, and 250 °C, and temperatures during welding were recorded with K-type thermocouples attached to the data acquisition. Several experiments including distortion, microstructure observation, hardness, and tensile testing were conducted. The results showed that increasing preheat temperature reduced welding distortion, with the best distortion reduction occurred at 250 °C. Preheating also caused microstructural changes in the weld metal region and heat affected zone (HAZ) with the amount of ferrite being increased with increasing preheating temperature. As a result, the ultimate tensile strength (UTS) of conventional weld metal, typically 642.94 MPa reduced to 547.64 MPa after preheating at temperature of 250 °C but this strength reduction is compensated by its improved ductility. The mechanisms of welding distortion and strengthening under preheating treatments are discussed in this paper.

Published:
May 31, 2025

Selection and Peer-review under the responsibility of the 6th BIS-STE 2024 Committee

Keywords

FCAW, A36 steel, Preheating, Distortion, Strength

Introduction

ASTM A36 structural steel finds massive applications in shipbuilding such as hulls and frames due to its high strength, typically 400-550 MPa, good formability and weldability. The good weldability of A36 steel is resulted from its low carbon content whereas the steel still maintains its strength by grain refinement according to Hall-Petch relationship. Welding is widely used for joining metals, especially in shipbuilding. This is because welding is able to create joints having high strength combined with good toughness, durability and efficiency. However, in the welding process on thin-wall plates, challenges often arise, such as distortion and residual stress caused by local heating [1]. The welding distortion affects the precision of the structures, structural integrity, and the appearance of ship components leading to the performance degradation [2]. As the result, additional works hence repair costs are required for correction. On the other hand, residual stress can cause embrittlement, stress corrosion cracking and reduced fatigue performance [3]. Ship structures are designed to withstand dynamic loads such as sea waves, cargo weight, and operational pressure over a long period of time [4]. As a consequence, a weld joint must meet stringent requirements to prevent failure in service.

One of the welding processes used in the fabrication of steel welded structures is flux-cored arc welding (FCAW). FCAW welding is commonly used in ship welding using CO_2 shielding gas with the solid wire being replaced by flux-cored wire. FCAW produces better penetration than GMAW because it does not require large heat input, thus providing better stress distribution around the weld joint [5,6]. Despite FCAW has many advantages, however the formation of distortion and residual stress can not be avoided by this type of welding technique. One of the distortion and residual stress elimination techniques is the preheating method.

During the past decade, there have been extensive research works on preheating to improve the quality of weld joints. According to Yurioka et al. [7], preheating is necessary to prevent cold cracks in steel welding by control of variables including the steel's chemical composition (CEN carbon equivalent), the amount of hydrogen in the weld metal, heat input, and plate thickness. Subsequently, Zubairuddin et al. [8], in their study, evaluated the effect of preheat during GTAW welding and showed that preheat produced a more homogeneous temperature distribution and significantly reduced residual stress and local deformation. Consistent with this report, Tariq et al. [9] and Jawad et al. [10] also reported that preheating ensured a slow cooling rate so that residual stress can be distributed widely and critical stress was reduced. The use of preheating also prevents the formation of a martensite structure, so that its hardness decreases and in contrast, the ductility of the weld increases. In addition, the slower cooling rate allows time for hydrogen to diffuse out of the weld metal prior to the formation of a hard and brittle microstructure, thus minimizing the risk of hydrogen-assisted cracking (HAC) [10,11].

In this study, preheating treatment was applied to FCAW process of A36 steel plates using preheating temperature of 100, 200, and 250 °C with objective of minimizing welding distortion. The mechanisms of distortion minimization under preheating treatment along with changes in the microstructures which affected mechanical properties such as hardness and tensile strength were evaluated.

Materials and Experimental Procedure

Materials

The materials used were ASTM A36 steel plates with the dimensions of 300 mm × 100 mm × 3 mm. The plates were welded using an automated flux cored arc welding (FCAW) with the flux cored wire of E71T-11. A butt joint having a single V-groove was selected with its groove angle of 70°, root face of 1 mm and gap of 1 mm. The chemical compositions of ASTM A36, E71T-11 flux core wire and weld metal are given in Table 1.

Table 1. Chemical composition of ASTM A36 plates, E71T-11 flux core wires and weld metal (wt.%)

Material	C	Si	Mn	P	S	Cr	Al	Cu	Ni	Mo	W	Ti	Nb	V	Fe
ASTM A36	0.14	0.23	0.73	0.02	0.03	0.04	0.03	0.01	0.01	0.01	0.00	0.00	0.00	0.00	Bal.
E71T-11	0.3	0.6	1.75	0.03	0.03	-	1.8	-	-	-	-	-	-	-	Bal.
Weld metal	0.26	0.63	0.56	0.00	0.00	0.02	0.91	0.01	0.01	0.00	0.00	0.00	0.00	0.00	Bal.

Welding Procedures

In this study, the FCAW processes were conducted automatically with the welding parameters and consumables used are given in Table 2. Figure 1a shows a schematic of conventional FCAW process with the welding parameters are given in Table 2. This FCAW process is often called "as welded condition" and it is used for the reference. The effects of preheating treatments were studied by placing two electric heater bands at both sides of the weld joint as shown in Figure 1b. Preheating temperatures of 100 °C, 200 °C, and 250 °C were selected in this study. The temperatures during welding process were monitored using K-type thermocouples at the distances of 10, 20 and 30 mm from the weld line.

Table 2. Consumables and welding parameters

Flux cored wires	:	E71T-11, Ø 0.8 mm
Wire feed speed	:	3.2 mm/s
Shielding gas	:	CO_2
Arc voltage	:	20 V
Welding current	:	110 A
Welding speed	:	1.5 mm/s
Welding Polarity	:	DCEN (Direct Current Electrode Negative)

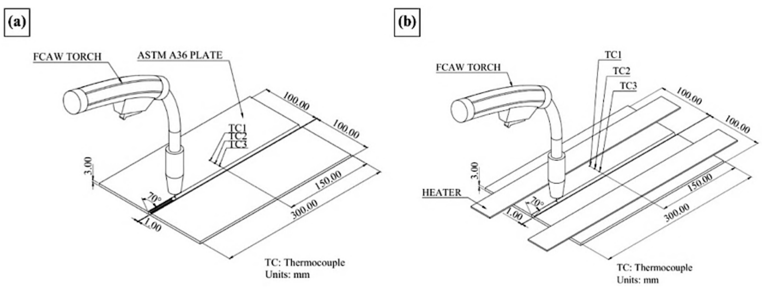

Figure 1. Schematic illustration of FCAW welding for: (a) as-welded, and (b) preheat treatment conditions

After welding, several experiments were conducted including distortion measurements, microstructural observations, hardness measurements and tensile strength tests. Detailed explanations of these experiments are described as the following.

Out-of-plane distortion measurements

After welding, the out-of-plane distortion for each welding condition was measured along the plate length, i.e. in the longitudinal direction at 10 mm-interval using a dial indicator. The measurements were taken in three locations, i.e. along the weld line and both sides of the welded plate.

Microstructure observation

The metallographic observations were focused on the cross-section of weld joints which consisted of weld metal (WM), heat-affected zone (HAZ), and base metal (BM). The specimens were first cut across the weld line and mounted in epoxy resin. Then grinding using emery paper from 100 grit to 5000 grit was performed followed by polishing and finally, etching using a Nital (2% HNO_3 + 98% propanol). Microstructural observations were devoted to the weld metal, heat-affected zone (HAZ), and base metal.

Microhardness measurements

The weld microhardness values across the entire zones of the weld joint were measured using Vickers microhardness as shown in Figure 2. The line of measurements was determined at a half thickness of the plate at the interval distance of 500 µm. The load, *F* and dwell time used for this investigation were 300 gf and 10 seconds respectively. The indentation diagonals, namely d_1 and d_2 were measured to determine the average diagonal value as given in Eq. (1).

$$D = \frac{d_1 + d_2}{2} \tag{1}$$

The Vickers microhardness (VHN) value for each point of measurements was calculated using Eq. (2), as follow:

$$VHN = \frac{1.854F}{D^2} \tag{2}$$

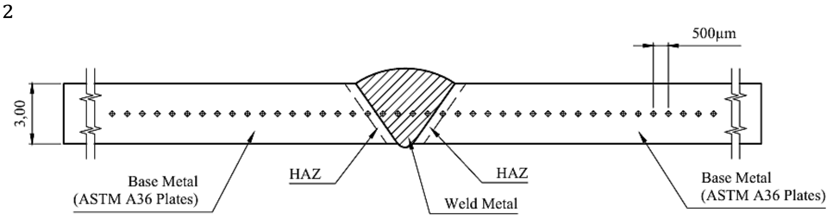

Figure 2. Illustration of Vickers microhardness test indentation marks

Tensile Test

The tensile test was performed along the longitudinal direction of the weld, following ASTM E8 standards. The dimensions of the weld specimen are illustrated in Figure 3. This test provided the tensile properties of both the weld metal and the base metal, including yield strength (YS) and ultimate tensile strength (UTS).

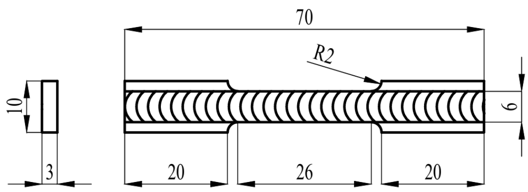

Figure 3. Longitudinal tensile test specimen

Results and Discussion

This section presents and discusses the findings of the study, focusing on the impact of preheating on distortion, tensile strength, and Vickers microhardness in ASTM A36 steel welded joints. The results include a comprehensive analysis of the mechanical properties, supported by SEM observations to understand the fracture surface characteristics. Each result is interpreted in relation to preheating temperatures to highlight the trends and their implications for welding performance.

Thermal cycles in welding

Figure 4 shows the weld thermal cycles under various conditions, taken at distances of 10 mm, 20 mm, and 30 mm from the weld centerline. As seen in Figure 4a, FCAW welding without treatment reaches a peak temperature of 550°C, as recorded by a thermocouple T_C1, which is the closest to the weld at 10 mm from the weld centerline. The weld joint in as-welded condition (Figure 4a) experiences a faster cooling rate compared to preheated welding, as shown in Figure 4b-d. There are two effects due to preheating. First, preheating increases the peak temperature and secondly, preheat slows down the cooling rate. These weld thermal cycles strongly influence the weld metal microstructure and hence mechanical properties.

Heat transfer during welding process of thin plates under preheating treatments can be explained by Rosenthal's equation as given in Eq. 3 below:

$$T - T_0 = \frac{q_w}{h(4\pi k\rho Ct)^{\frac{1}{2}}} \exp\left(-\frac{r^2}{4\alpha t}\right) \tag{3}$$

where q_w is heat input determined by calculating *(Q/v)*, *Q* is heat energy, *v* is welding speed, T_o is temperature at the start of welding process, *(ρC)* is specific heat per unit volume, k is thermal conductivity, a is thermal diffusivity which is equivalent to *k/(ρC)*, *h* is the plate thickness, *r* is radial/lateral distance from the weld and *t* is time. According to Eq. (3), as preheating temperature, namely *To* increases, the peak temperature increases as well. Nevertheless, preheating can help to reduce extreme temperature gradients between the weld area and its surroundings, enabling more uniform heat distribution. Additionally, preheating retains heat longer and prevents rapid cooling, thereby reducing the risk of cracking due to high thermal stress [10,11,12].

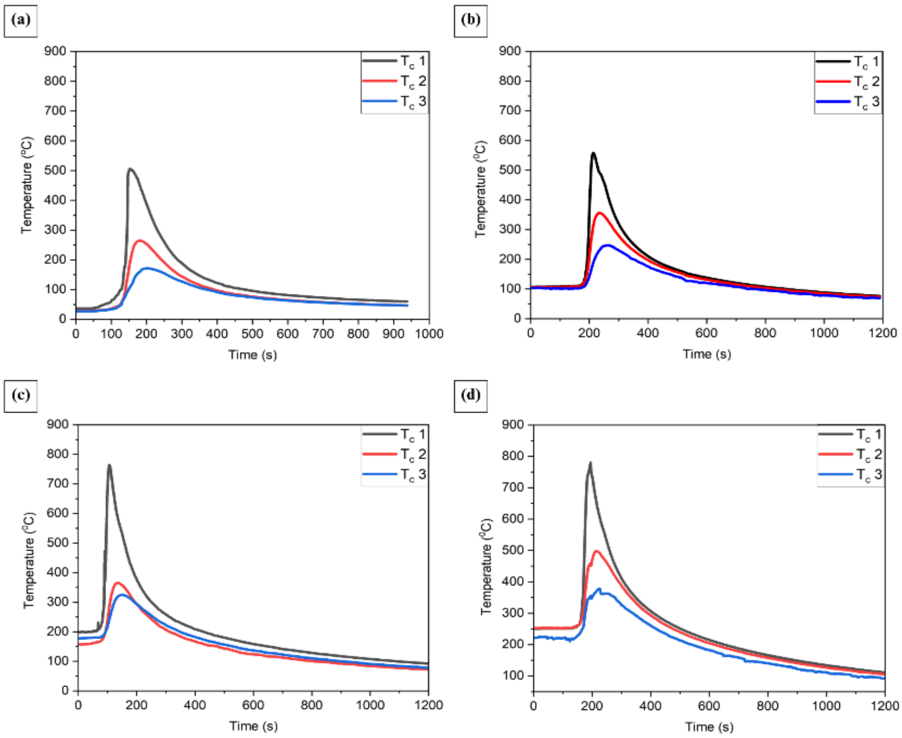

Figure 4. Weld thermal cycles for: (a) as-welded, (b) preheat-100°C, (c) preheat-200°C, and (d) preheat-250°C.

Weld distortion measurements

The results of the out-of-plane distortion measurements are shown in Figure 5. This distortion occurs during the flux-cored arc welding process and is measured in the longitudinal direction. As seen in Figure 5, the highest weld distortion occurs in as-welded condition, while the use of preheating gradually reduces distortion. In as welded condition, heat from welding increases temperature around the weld zone so that a significant temperature difference arises between the weld zone and the base material. This high-temperature gradient creates uneven thermal contraction during welding, resulting in significant deformation as the material cools. In addition, rapid cooling also generates high thermal stresses, leading to severe distortion and an increased risk of cracking due to high residual stress [9,12]. Preheating, on the other hand, controls the cooling rate, thereby reducing the thermal stress experienced by the material due to a more uniform temperature distribution.

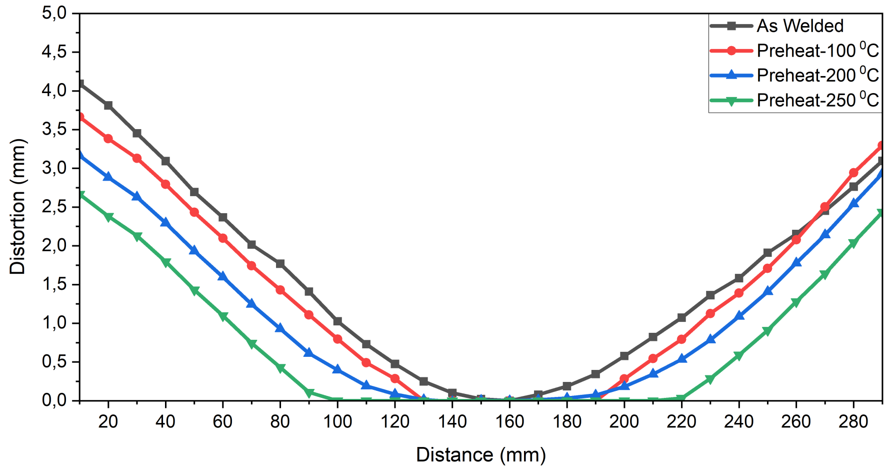

Figure 5. Out-of-plane distortions in the welded plates.

Based on the results of welding distortion measurements in Figure 6a, the occurrence of welding distortion in as welded condition is proposed as the following. As the weld metal region and its surrounding region cool, the compressive longitudinal thermal stress, σ_s is formed with its magnitude is given by Eq. (4). [13] :

$$\sigma_s = \mu_l \frac{\alpha q_w}{\rho C A} E \tag{4}$$

where q_w is heat input which is heat energy (q) divided by welding speed (v), C is heat capacity, A is cross-section area of weld, μ_l is longitudinal stiffness factor, α is coefficient of thermal expansion, ρ is density, E is Young's modulus of elasticity. Furthermore, longitudinal out-of-plane distortion often known as buckling distortion is created as the shrinkage stress, σ_s exceeds the critical buckling stress. In the case of the welded plate, the value of σ_{cr} is determined by [14] :

$$\sigma_{cr} = k \frac{\pi^2 E h^2}{12(1-v^2)w^2} \tag{5}$$

where h is plate thickness, w is plate width and k is constant.

Weld microstructures

Figure 6 shows microstructures of the weld metals with and without preheating treatments. In as-welded condition in which rapid cooling occurs as shown in Figure 6a, the microstructure is dominated by bainite and hard, brittle martensite combined with continuous networks of grain boundary ferrite which appears bright. Meanwhile, Figure 6b-d illustrate the preheated welds that experience significantly slower cooling rates. As a result, the percentages of grain boundary ferrite and Widmanstatten ferrite increase at the expense of martensite in preheating conditions. It is confirmed that the amount of grain boundary ferrite and Widmanstatten ferrite increase with increasing preheating temperatures. It is well known that ferrites are more ductile and crack-resistant, hence providing better toughness.

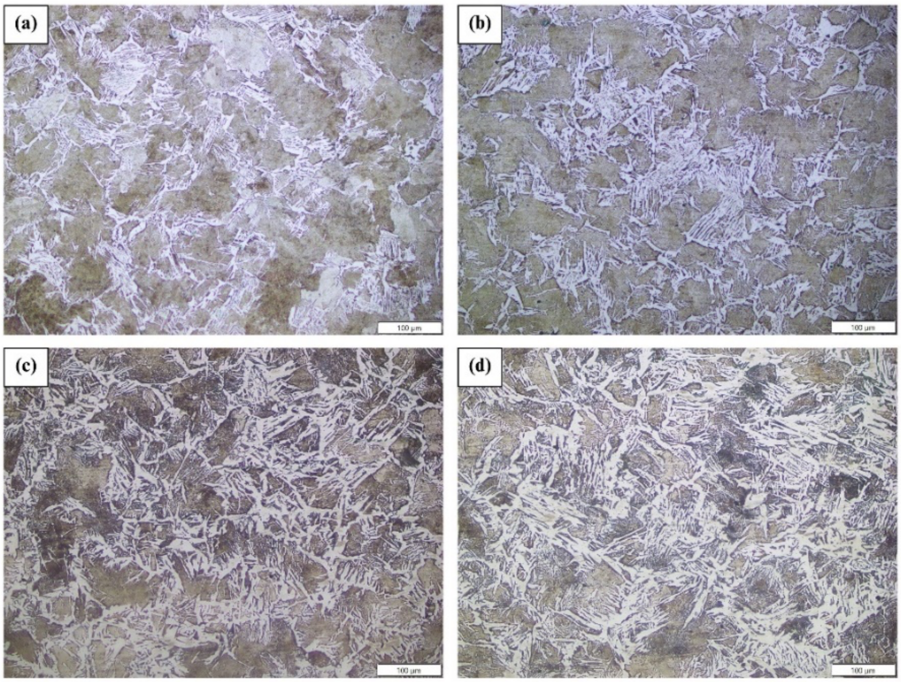

Figure 6. Weld microstructures in: (a) as-welded, and (b),(c),(d) preheating conditions at 100°C, 200°C, and 250°C respectively

The formation of grain boundary ferrite in Figure 6 reveals two types of growth, i.e. lengthening along grain boundaries and thickening towards the prior austenitic grains. The growth of thickening (x) is controlled by diffusion during austenite (γ) to ferrite (α) phase transformation and it is given by [15,16]:

$$x = \frac{(C_\gamma - C_o)}{[(C_\gamma - C_\alpha)(C_o - C_\alpha)]^{1/2}}(Dt)^{1/2} \tag{6}$$

where *x* is half thickness, *t* is time, *D* is diffusion coefficient of C in γ, C_o is concentration of C in the weld metal, C_γ is concentration of C in γ at the interface, C_α : concentration of C in α at the interface. Based on Eq. (6), it is seen that the growth of thickening is linearly proportional to $t^{1/2}$ suggesting that the growth of thickening is slow. As a result, the grain boundary ferrite can not completely occupy the austenite grains during the γ→α transformation.

Figure 7a shows the HAZ microstructure in as-welded condition which is composed of martensite as the matrix surrounded by coarse grain boundaries due to rapid cooling [11,17]. Some Widmanstatten ferrite plates are formed within the grains. The introduction of preheating at 100 °C increases the percentages of grain boundary ferrite and Widmanstatten ferrite as shown in Figure 7b. Further increase in preheating temperature to 200 °C as shown in Figure 7c suppresses the formation of matrix due to slower cooling rate in favor of Widmanstatten ferrite and fully developed grain boundary and Widmanstatten ferrites are observed at preheating temperature of 250 °C.

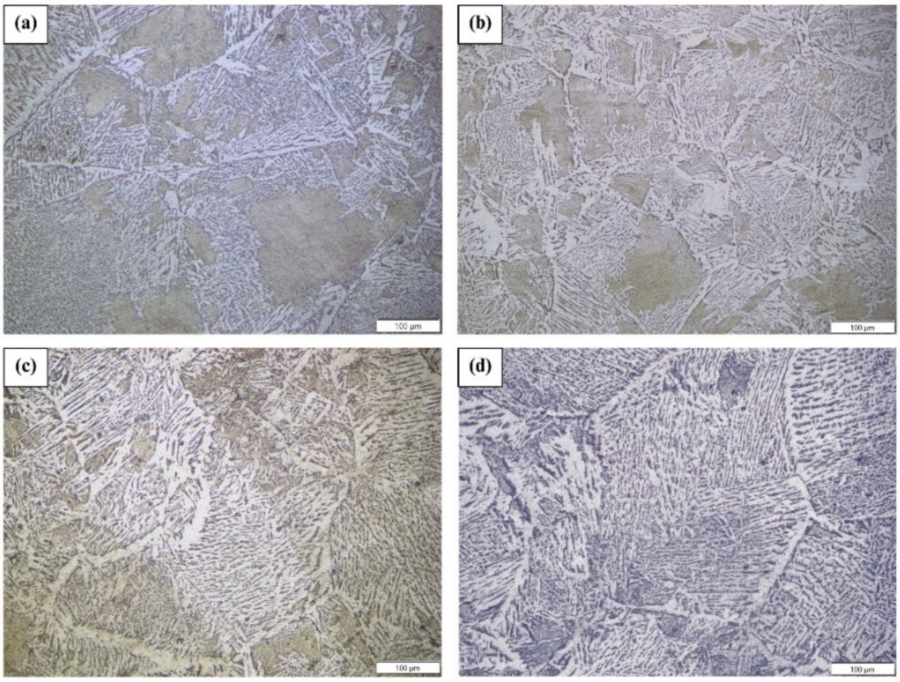

Figure 7. Heat affected zone (HAZ) microstructures in: (a) as-welded, and (b),(c),(d) preheating conditions at 100°C, 200°C, and 250°C respectively

Hardness distributions

The results of the Vickers microhardness measurements are shown in Figure 8. It can be seen that the weld joint in as-welded condition shows high hardness with the maximum hardness, typically 284 HV is achieved in the weld metal region. This high hardness is attributed to the rapid cooling after welding, which promotes the formation of a martensitic microstructure in the weld area and the Heat Affected Zone (HAZ). Martensite is known for its high hardness but is brittle hence increasing the risk of cracking. With the application of preheating at 100°C, the average hardness in the weld metal region decreases to 211 HV. This is because preheating slows down the cooling rate, preventing excessive martensite formation and encouraging the development of more stable and softer grain boundary ferrite and Widmanstatten ferrite structures. At a higher preheating temperature that is 200°C, the hardness further decreases to 199 HV due to further decrease in the cooling rate. The dominant grain boundary and Widmanstatten ferrite structures in the weld area provide better ductility and improves resistance to plastic deformation. At 250°C, the hardness of weld metal region reaches the lowest value, i.e. 194 HV. Preheating at this temperature ensures highly controlled cooling, resulting in a microstructure almost entirely composed of grain boundary and Widmanstatten ferrites. This significantly reduces the hardness but increases material ductility.

It is summarized that the increase in preheat temperature from 100°C to 250°C results in a significant decrease in Vickers hardness values. This demonstrates that preheating effectively controls the cooling rate and prevents the formation of hard microstructures like martensite, producing softer and more ductile material [10,13]. This condition is crucial for reducing the risk of cracking due to residual stress and improving the weld joint's resistance to dynamic loads.

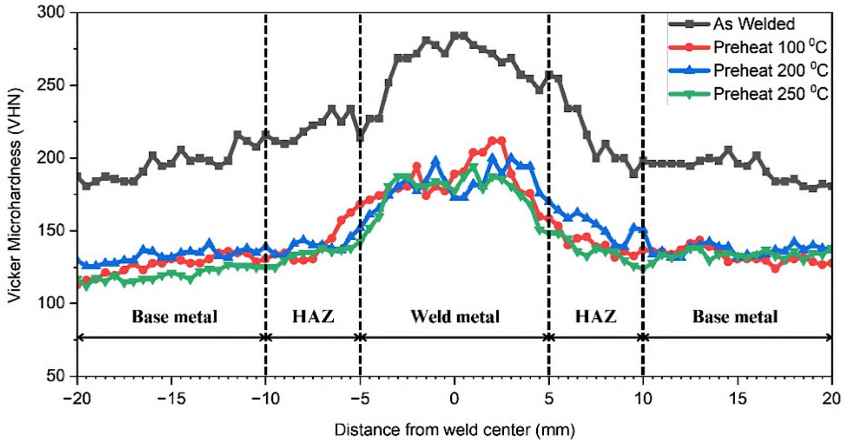

Figure 8. Hardness distributions

Tensile strengths

Figure 9 shows the tensile test results of weld metal region with and without preheating presented in the tensile strength and yield strength. In as-welded condition, the tensile strength of weld metal reaches 642.94 MPa whereas the value of yield strength is 462.08 MPa. This high tensile and yield strength is due to the rapid cooling after welding, which promotes the formation of hard microstructures like martensite in the weld zone and HAZ. However, this type of microstructure is brittle and exhibits low ductility. The introduction of preheating at 100°C causes the tensile strength to decrease to 616.86 MPa, while the yield stress drops to 430.21 MPa. At a higher preheating temperature of 200°C, the tensile strength further decreases to 558.21 MPa, and the yield strength drops to 398.12 MPa. At very high preheating temperature, typically 250°C results in the lowest tensile strength of 547.64 MPa, with a yield strength of 393.83 MPa

Based on these results, it is concluded that the tensile strength and yield strength decrease with increasing preheat temperature. This is attributed to the slower cooling rate, which inhibits the formation of hard microstructures like martensite in favour of ferrite structures [10,13]. The reduction in tensile strength is compensated by an improvement in ductility, which is required for preventing failure under dynamic loads in structural applications such as shipbuilding.

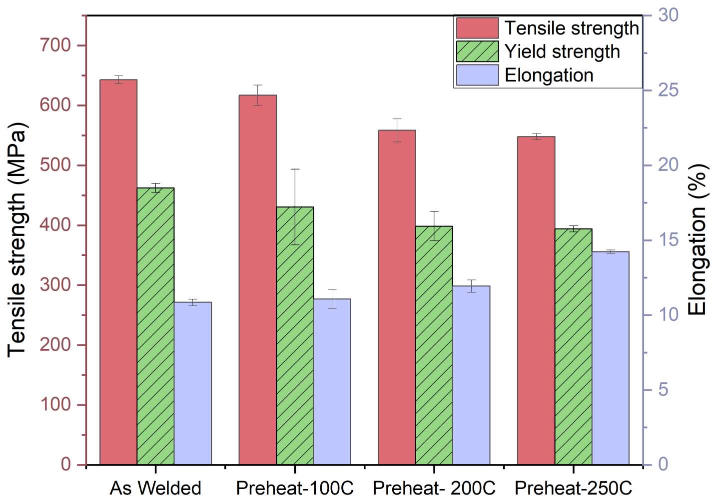

Figure 9. Tensile properties of the weld joints under study.

SEM Fracture Analysis

Figure 10 shows the results of scanning electron microscopy (SEM) fracture analysis after tensile tests reveal significant differences between the as-welded condition and preheat condition at 250°C. In the as-welded condition, the fracture surface is dominated by large and deep dimples, which are characteristic of ductile fracture. These dimples are formed due to significant plastic deformation before fracture occurs. However, the rapid cooling rate in the as-welded condition promotes the formation of hard microstructures such as martensite in the weld zone and HAZ. While this rapid cooling increases the hardness, but it reduces the ductility of the material, making the weld metal and HAZ more susceptible to cracking under static and repeated loads.

In contrast, the fracture surface in the preheat condition at 250°C exhibits smaller and shallower dimples. This indicates that preheating at 250°C slows the cooling rate, reducing martensite formation and encouraging the development of more stable and softer grain boundary and Widmanstatten ferrite structures. The more homogeneous microstructure enhances the material’s ductility, allowing for more uniform plastic deformation and a more controlled fracture mechanism. The smaller dimples suggest that the energy absorbed during plastic deformation is more evenly distributed, resulting in a more stable fracture process.

These differences in dimple structures between the as-welded and 250°C-preheat conditions demonstrate that preheating effectively reduces thermal stress and prevents rapid cooling. This contributes to improved ductility of the welded joint and reduced hardness, which are crucial for enhancing the material's resistance to failure under static and dynamic loads.

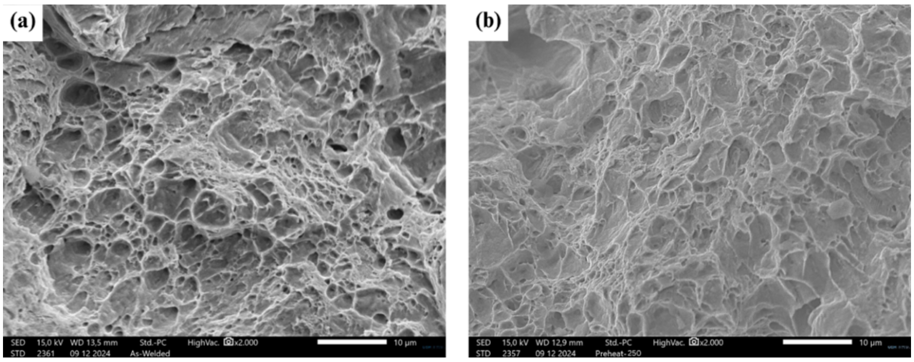

Figure 10. SEM fractographs of the weld joints in: (a) as-welded, and (b) preheat-250°C conditions.

Conclusion

Based on the results of the present investigation, some conclusions are drawn as follows:

a. Microstructure in the weld metal region of FCAWed A36 steel joints is marked by continuous networks of grain boundary ferrite in the matrix martensite. The use of preheating increases the amount of grain boundary ferrite and another microstructure known as Widmanstatten ferrite is formed.
b. Increasing preheating temperature causes the grains in HAZ to become larger accompanied by Widmanstatten ferrites which form within the grains.
c. The hardness in the weld metal and HAZ are decreased due to formation of grain boundary ferrite and Widmanstatten ferrite at the expense of martensitic structure.
d. The ultimate tensile strength (UTS) and yield strength (YS) of the FCAW joints are reduced under preheating treatment but the ductility increases.
e. Preheating can reduce the out-of-plane distortion and increasing preheating temperature effectively minimize the distortion.

Acknowledgments

The authors would like to express their sincere gratitude to the Materials Engineering Laboratory, Universitas Gadjah Mada, for providing the facilities required for this study. Special thanks are also extended to the Vocational School Laboratory, Universitas Gadjah Mada, for their assistance in conducting the SEM analysis.

References

[1] S. Hernandez Palacio, M. Cardona Castaño, and J. E. Giraldo Barred, “Construction of productivity windows for fillet welds using the FCAW process for thin ship panel manufacturing,” *Cienc. y Tecnol. buques*, vol. 12, no. 24, p. 17, 2019, doi: 10.25043/19098642.176.
[2] E. Education, M. R. Goyal, and E. W. Harmsen, “Principles and Applications for Principles and Applications for,” vol. 4, pp. 0–471, 1999.
[3] Y. P. Yang, “Recent Advances in Prediction of Weld Residual Stress and Distortion — Part 2,” *Weld. J.*, vol. 100, no. 6, pp. 193S-206S, 2021, doi: 10.29391/2021.100.016.
[4] P. Corigliano, F. Frisone, C. Chianese, M. Altosole, V. Piscopo, and A. Scamardella, “Fatigue Overview of Ship Structures under Induced Wave Loads,” *J. Mar. Sci. Eng.*, vol. 12, no. 9, p. 1608, 2024, doi:

10.3390/jmse12091608.
[5] R. Boekholt, “The use of semi-automatic and automatic GMAW and FCAW in shipbuilding,” *Weld. Mech. Autom. Shipbuild. Worldw.*, pp. 103–131, 1996, doi: 10.1533/9780857093196.103.
[6] M. S. da Silva, D. Souza, E. H. de Lima, K. E. Bianchi, and L. O. Vilarinho, “Analysis of fatigue-related aspects of FCAW and GMAW butt-welded joints in a structural steel,” *J. Brazilian Soc. Mech. Sci. Eng.*, vol. 42, no. 1, pp. 1–13, 2020, doi: 10.1007/s40430-019-2142-8.
[7] N. Yurioka and T. Kasuya, “A Chart Method to Determine Necessary Preheat Temperature in Steel Welding,” *Q. J. Japan Weld. Soc.*, vol. 13, no. 3, pp. 347–357, 1995, doi: 10.2207/qjjws.13.347.
[8] M. Zubairuddin, S. K. Albert, M. Vasudevan, S. Mahadevan, V. Chaudhri, and V. K. Suri, “Thermomechanical analysis of preheat effect on grade P91 steel during GTA welding,” *Mater. Manuf. Process.*, vol. 31, no. 3, pp. 366–371, 2016, doi: 10.1080/10426914.2015.1025964.
[9] U. Tariq, S. H. Wu, M. A. Mahmood, M. M. Woodworth, and F. Liou, “Effect of Pre-Heating on Residual Stresses and Deformation in Laser-Based Directed Energy Deposition Repair: A Comparative Analysis,” *Materials (Basel).*, vol. 17, no. 10, 2024, doi: 10.3390/ma17102179.
[10] M. Jawad *et al.*, “Revealing the microstructure and mechanical attributes of pre-heated conditions for gas tungsten arc welded AISI 1045 steel joints,” *Int. J. Press. Vessel. Pip.*, vol. 192, no. May, p. 104440, 2021, doi: 10.1016/j.ijpvp.2021.104440.
[11] G. K. Padhy, V. Ramasubbu, N. Murugesan, C. Remash, and S. K. Albert, “Effect of preheat and post-heating on diffusible hydrogen content of welds,” *Sci. Technol. Weld. Join.*, vol. 17, no. 5, pp. 408–413, 2012, doi: 10.1179/1362171812Y.0000000023.
[12] G. Chakraborty, R. Rejeesh, M. Zubairuddin, and S. K. Albert, “Effect of preheating and post heating in reducing diffusible hydrogen content and hydrogen assisted cracking susceptibility of modified 9Cr–1Mo steel,” *Sci. Technol. Weld. Join.*, vol. 25, no. 8, pp. 637–643, 2020, doi: 10.1080/13621718.2020.1796251.
[13] D. Radaj, *Heat effects of welding, Springer-Verlag, Berlin,*. 1992.
[14] Y. P. Yang and P. Dong, “Buckling distortions and mitigation techniques for thin-section structures,” *J. Mater. Eng. Perform.*, vol. 21, no. 2, pp. 153–160, 2012, doi: 10.1007/s11665-011-9928-x.
[15] Bhadeshia, Harshad Kumar Dharamshi Hansraj, and Robert William Kerr Honeycombe, *Steels : microstructure and properties / H.K.D.H. Bhadeshia and Robert Honeycombe.*, 3rd ed. Amsterdam ; Boston: Elsevier, Butterworth-Heinemann, 2006.
[16] M. N. Ilman and Sehono, *Ilmu dan Teknologi Pengelasan*. Yogyakarta: UGM PRESS, 2023.
[17] M. N. Ilman, Kusmono, M. R. Muslih, N. A. Triwibowo, and Sehono, “Enhanced fatigue performance of tandem MIG 5083 aluminium alloy weld joints by heat sink and static thermal tensioning,” *Int. J. Light. Mater. Manuf.*, vol. 5, no. 4, pp. 440–452, 2022, doi: 10.1016/j.ijlmm.2022.05.003.